PAPER

Check for updates

Acidity modifications of nanozeolite-Y for enhanced selectivity to olefins from the steam catalytic cracking of dodecane†

Emad N. Shafei,[a] Ahmad Masudi,*[b] Zain H. Yamani [iD] [b] and Oki Muraza [iD] *[b]

Nanozeolite-Y was synthesized in the absence of a templating agent with several modification methods. The parent nanozeolite-Y was prepared with different sodium (Na) contents and crystallization conditions. Then, the parent nanozeolite-Y was modified by ion exchange, calcination, and steam treatment. The treatment caused insignificant changes to the ratio of alumina and silica but altered the zeolite acid sites. The Lewis and Brønsted acidity changed after the treatment depending on the modification approach, as indicated by the FTIR spectroscopy of pyridine. The ammonia temperature programmed desorption (NH_3-TPD) confirmed that the acid sites consisted of weak and medium sites, which decreased after modifications. Moreover, the solid-state nuclear magnetic resonance (NMR) spectroscopy revealed that the position of Al shifted from tetrahedral to a combined octahedral and pentahedral framework. The catalytic evaluation for dodecane cracking at 550 °C shows the gas yield as the main product with naphtha as a side product. The gas yield consisted of 50% light olefins from ethylene to butene. However, the process yielded 9% of coke that led to faster catalyst deactivation because of nanozeolite-Y evolution and product transformation.

Introduction

The demand for olefins has shown an increasing trend in recent times. Light olefins from ethylene to butene considered as the most valuable feedstock with improving living standard and elevating need to polymers.[1] Most olefins in the market are produced from naphtha steam cracking and petrochemical products from oil refinery. However, there is an increasing trend to replace the heavy liquid hydrocarbon feed by ethane as a feed in modern steam crackers.[2] As a result, there is gap between demand and production to light olefins. Based on experience from the shale gas industry, new resources with a better technology are required to improve the efficiency of chemical production.[3] In recent years, there is a growing interest to produce chemicals from heavy oil. However, heavy oil processing is more challenging due to its higher viscosity and longer chains. As a representative of long chain hydrocarbons, *n*-dodecane ($C_{12}H_{26}$) was used to understand the catalytic activities of heavy oil before any further studies.[4]

At the moment, some researchers have also conducted in-depth studies on biomass valorization to fuel and chemicals.

In accordance to environmental concerns, the technological barriers have been minimized by mimicking the process in oil refinery.[5] Pyrolysis is considered as one of the promising routes to produce numerous value-added chemicals. In pyrolysis, *n*-dodecane is the preferred product in the production of bio-oil.[6] In addition, *n*-dodecane is also a derivative product of lauric acid, one of the important fatty acids in biomass conversion.[7] Thus, *n*-dodecane transformation is a feedstock intersection between heavy oil and biomass conversion.

n-Dodecane conversion can be conducted using various heterogeneous catalysts. Zeolitic-based materials are the common catalyst in the petrochemical industry with the ability to generate several products through simple or complex stages. The zeolitic catalysts exhibit controllable porosity with fine tuning acidity that plays a crucial role in cracking long hydrocarbons through carbenium intermediates.[8,9] However, the utilization of conventional zeolites is constrained with slow mass transfer and rapid coke deactivation. Conventional zeolite Y has supercages with a diameter of 12 Å, but the pore opening is constrained with an oxygen ring with a diameter of 7.4 Å.[10,11] Although the catalytic reaction may occur in the internal and external sites, it is limited to molecules with bigger sizes. Big molecules were cracked only in the external sites that generated more coke and decreased the catalyst performance.[12]

Nanosized zeolite is a promising catalyst to overcome previous limitations due to its higher ratio of external to internal sites. There are two general approaches to synthesizing nanozeolite, namely top-down and bottom-up.[13] The bottom-up

[a]Research and Development Center, Saudi Aramco, Dhahran 31311, Saudi Arabia

[b]Interdisciplinary Research Center for Hydrogen and Energy Storage and Chemical Engineering Department King Fahd University of Petroleum & Minerals, Dhahran 31261, Saudi Arabia. E-mail: omuraza@kfupm.edu.sa; oki.muraza@pertamina.com

approach is favorable as it exhibits lower agglomeration and easier acidity control. Vuong *et al.*[14] used an organic solvent to synthesize zeolite Y for gas oil catalytic cracking that had the smallest crystal size of 25 nm. Moreover, Radman *et al.* prepared a similar nanozeolite type material with a crystallite size of 60 nm without a template.[15] Nevertheless, there are still limited studies on the production of nanozeolites in the absence of a template with a crystal size lower than 15 nm.

To the best of our knowledge, nanozeolite Y acidity modification as one of the influencing parameters in *n*-dodecane cracking is rarely reported in literature. Ahmed *et al.* reported that acidity and pore entrance played a crucial role in the enhancement of olefins yield using EU-1 and ZSM-48.[16] Hawkins *et al.* used a steam treatment to modify ZSM-5 properties and confirmed that the treatment significantly changed the acidity. Previously, it was reported that hierarchical zeolite increased olefin selectivity[17] using the dual templating agent of hierarchical ZSM-5.[18] In this study, the effect of nanozeolite Y acidity to olefin selectivity was elucidated. The acidity modification was conducted using three facile approaches from the parent nanozeolite-Y, namely ion exchange, calcination, and steam treatment. In addition, coke formation in the catalyst was also studied in an attempt to extend the catalyst lifetime in the future.

Experimental

Materials

Sodium hydroxide (NaOH, 97%) was purchased from Sigma-Aldrich, aluminum powder (Al, 325 mesh., >98%) was obtained from Loba Chemie. Moreover, aluminum hydroxide (Al(OH)$_3$, 90%) and colloidal silica (Ludox-HS 30, 40 wt% SiO$_2$) were obtained from Panreac and Sigma-Aldrich, respectively. Ammonium nitrate (NH$_4$NO$_3$) and iso-propanol were purchased from Merck.

Synthesis of nanosized zeolite Y

The nanosized zeolite Y was produced using a template-free approach with modification from Awala *et al.*[19] There are two types of nanozeolite parents in this study namely, NaY-10 and NaY 70. The preparation of NaY-10 with a molar composition of 9Na$_2$O:0.7Al$_2$O$_3$:10SiO$_2$:160H$_2$O was conducted as follows: 19 g of NaOH was dissolved in 38 g of water, followed by the addition of Al powder with constant stirring, as aluminate source (solution A). Moreover, for the source of silica (solution B), 71 g of colloidal silica was added to a NaOH solution with constant stirring. The resultant turbid white suspension was placed in a milestone microwave at 800 W with 4 min heating to reach 100 °C, then maintained for 1 min. The solution B was kept under vigorous stirring (1100 rpm) in an ice bath with the slow addition of solution A. The resulted solution was left to age at room temperature under constant stirring at 700 rpm for 24 h. Then, the hydrothermal treatment was performed at 50 °C for 45 h. The produced slurry was washed, centrifuged several times, and then dried overnight at 105 °C. Moreover, the parent NaY-70 was synthesized based on a chemical composition of

8Na$_2$O:0.7Al$_2$O$_3$:10SiO$_2$:160H$_2$O with hydrothermal treatment at 120 °C for 70 min.

Nanozeolite Y modification

There are three modifications of the parent nanozeolite Y in this study namely, ion exchange (NH$_4$–Y10), calcination (H–Y10) and steam treatment (S–Y10). The preparation of NH$_4$Y was carried out by adding 2 mmol of NH$_4$NO$_3$ to 1 g of the parent Nanozeolite Y powder. Initially, the NH$_4$NO$_3$ solution was heated to 80 °C, and then the zeolite powder was added with vigorous stirring for 3 h. The suspension was then centrifuged and washed with distilled water. This ionic exchange treatment was repeated three times. The solid slurry was washed with iso-propanol, centrifuged, and dried at 105 °C overnight to produce NH$_4$–Y powder. After that, the protonated nanozeolite-Y (H–Y) was obtained after the calcination of NH$_4$Y at 550 °C for 4 h. Moreover, S–Y was acquired by the steam treatment of NH$_4$–Y at 600 °C for 7 h under a nitrogen flow.

Characterization

The prepared zeolite samples were characterized using powder X-ray diffraction (XRD), field emission-scanning electron microscopy (FESEM), X-ray fluorescence (XRF), FTIR pyridine, nuclear magnetic resonance (NMR), ammonia temperature programmed desorption (NH$_3$-TPD) and thermogravimetry (TG).

The samples crystallinities and purities were verified with a Rigaku XRD in the range of 5–50° at a step size of 0.03°. This instrument used CuKα radiation ($\lambda = 1.5406$ Å), and the data were analysed with the EVA 8.0 (Rigaku Miniflex) software. The sample morphologies were observed *via* FESEM having a low acceleration voltage (LYRA 3 Dual Beam Tescan). The atomic content was detected by XRF.

The acid nature of the catalysts was determined with pyridine adsorption. Moreover, the acidity strength was evaluated with NH$_3$-TPD. The pyridine adsorption was conducted with a NICOLET 6700 FTIR equipped with a MCT detector. A pellet form of the zeolite sample was treated in a vacuum at 550 °C for 1 h and placed in a ZnSe cell. Pyridine was introduced as a probe molecule for 10 min after cooling down the sample to 150 °C, and then the pyridine was removed under vacuum conditions at the same temperature. The amount of acid sites was calculated using an equation described in literature.[20] Thereafter, the acidity distribution was verified by NH$_3$-TPD Micrometrics AutoChem II. The measurement was conducted by purging the sample surface with helium gas at 300 °C, followed by a treatment with ammonia at 100 °C for 30 min. Finally, the adsorbed ammonia was removed by increasing the temperature to 500 °C.

The distribution and structure of an atom can be elucidated *via* solid state nuclear magnetic resonance (NMR). In this study, solid state ^{27}Al MAS NMR of the catalysts were conducted using a JEOL ECA-600 at a resonance frequency of 156.4 MHz to identify the Al structure after each treatment. This instrument has 4 mm of the rotor sample. Moreover, the amount of coke was monitored by thermogravimetry (TG) in the range of 400–800 °C by measuring weight loss during the heating treatment.

Catalytic evaluation

The catalytic activity of the as-prepared zeolite catalysts was evaluated under the assistance of steam. The process was conducted in a packed-bed reactor to crack dodecane at 550 °C. In this study, time on stream (TOS) and hourly space velocity were fixed at 1 h and 1 h^{-1}, respectively. Nitrogen was used as the gas carrier, while the product distribution was determined *via* GC-MS. The experimental set up of this study is shown in Fig. 1.

Results and discussion

Synthesis of nano-sized zeolite Y

Zeolite properties play a role in determining the catalytic activity, thus making the synthesis part a center of interest for improving the catalytic performance. Camblor *et al.*[21] were among the first researchers to successfully prepare nanozeolite Y, which was then improved by Landau *et al.*, confirming the better activity of nanosized zeolite.[22] Radman *et al.* recently produced nanozeolite Y in the absence of a template and found that the crystal size depended on the metal alkali content.[15] There are two parent nanozeolite Ys in this study namely, NaY-10 and NaY-70, with different contents of Na and hydrothermal conditions. Fig. 2 shows the XRD pattern of the catalysts, which is similar to that of the FAU zeolite, as reported in literature (JCPDS number 01-077-1551), indicating its pure crystallinity.[19] The diffractogram only showed different intensities as a sign of different crystallinity and crystallite sizes. NaY-10 exhibited lower crystallinity and broader peak with a crystallite size of 10 nm. Moreover, NaY-70 has a bigger crystallite size of 70 nm. This result was also supported by the FESEM images, as displayed in Fig. 3, with semi-spherical shapes and smaller size of NaY-10. Thus, NaY-10 was chosen as the parent nanozeolite Y for further modifications.

The modification of nanozeolite Y was conducted by ionic exchange, calcination, and steam. Then, the crystal structure
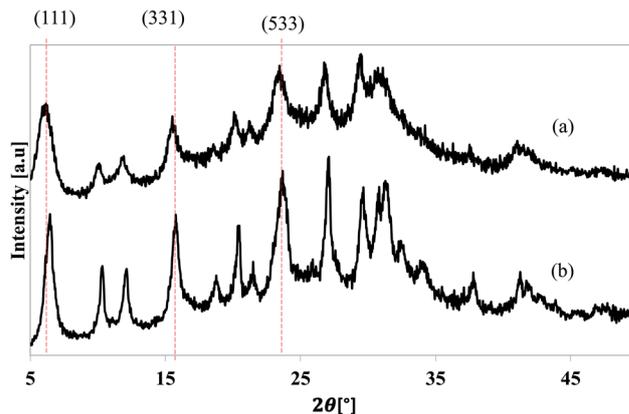

Fig. 2 FAU XRD patterns of (a) Na–Y10 (b) Na–Y70.

and morphology were identified. From Fig. S1 and S2,† it clearly observed that there was a significant change in the XRD pattern after the steaming treatment due to several factors such as sintering, structural collapse and generation of an amorphous phase.[23]

The atomic composition of the nanozeolite Y was quantified by XRF, and the results are listed in Table 1. The parent nanozeolite Y shows a silica to alumina ratio (Si/Al) of 2.0, which became 1.8–2.2 after the treatment. This result implied that the treatment had a minimal impact on the silica–alumina content of the parent nanozeolite-Y.[24]

The elucidation of the acid characteristic was crucial in the catalysis area, particularly in catalytic cracking. The nature and acid distribution should be comprehended to improve the efficiency of the targeted reactions. In general, the acidity of a zeolite can be determined by both NH$_3$ TPD and pyridine adsorption. A zeolite has both Lewis and Brønsted acid sites, which are differentiated by pyridine adsorption, while NH$_3$ TPD is beneficial in characterizing the acidity strength. However,
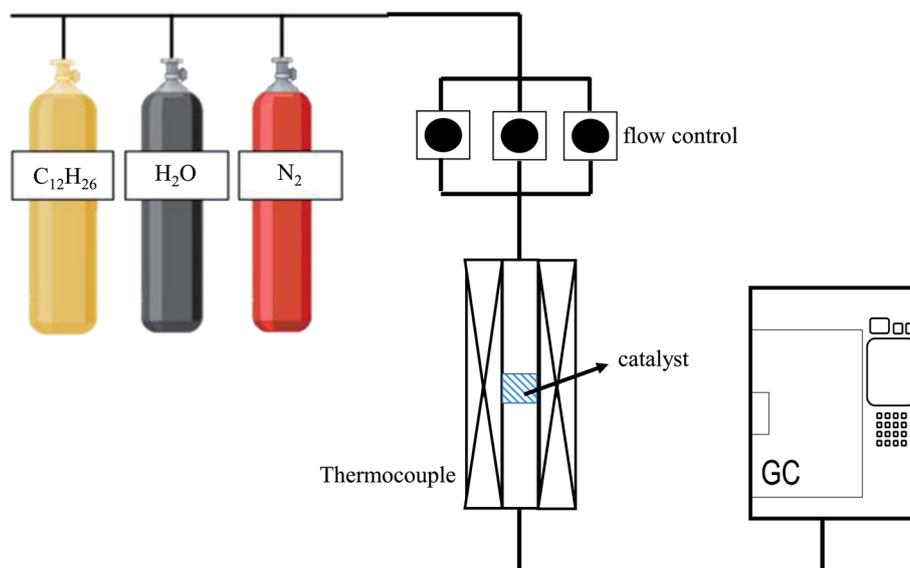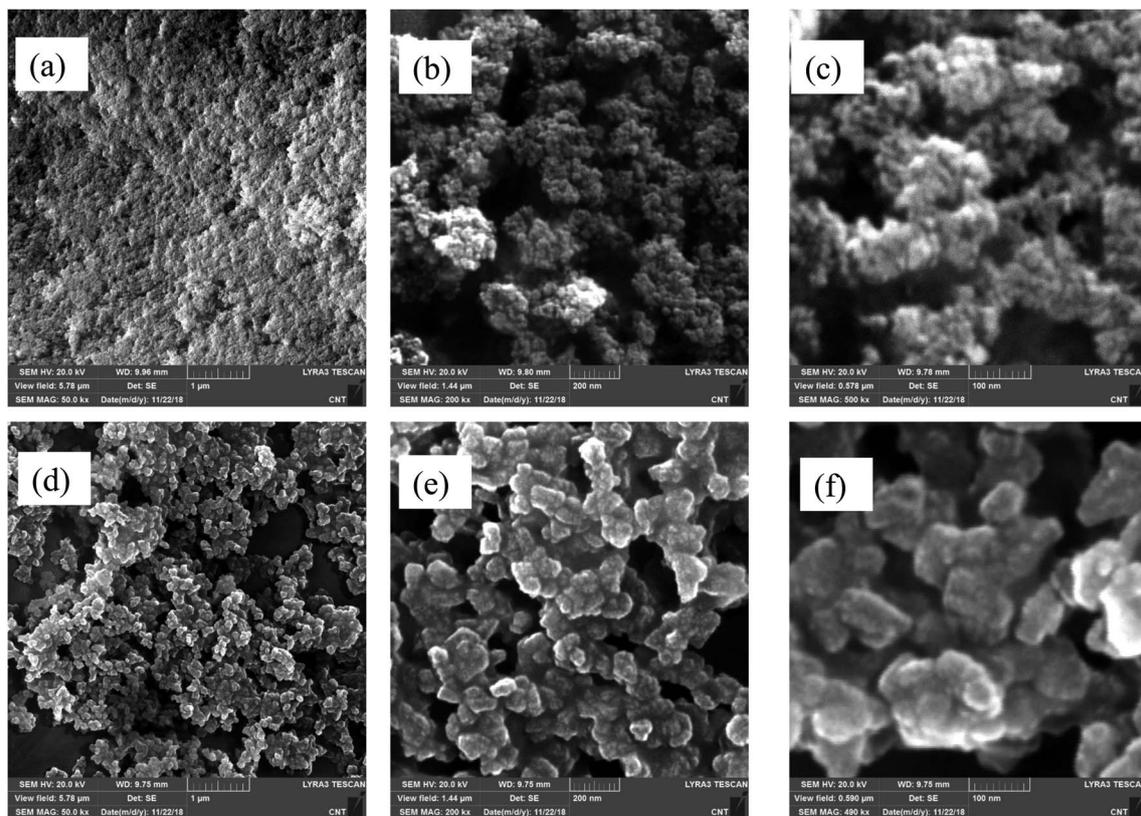

Fig. 1 Steam dodecane cracking process.

Fig. 3 FAU FESEM images of Na−Y10 (a−c) and Na−Y70 (d−f).

Table 1 XRF, pyridine FTIR and NH$_3$-TPD analysis of nanozeolite (a) NH$_4$Y10 (b) H−Y10 (c) SY-10 and (d) Y 10 coke

| Sample | Na (wt%) | Si/Al | Pyridine FTIR | | | | Total NH$_3$ adsorption (μmol g^{-1}) |
			Total acid sites (mmol g^{-1})	Brønsted acid sites (mmol g^{-1})	Lewis acid sites (mmol g^{-1})	Area$_{BA}$/area$_{LA}$	
NH$_4$−Y10	11	2.0	0.12	0.08	0.04	1.70	968.9
H−Y10	7.99	1.8	0.43	0.23	0.20	1.17	592.5
S−Y10	5.65	1.9	0.60	0.25	0.35	0.73	294.3
S−Y10 coke	8.08	2.2					148.4

prior to the acidity measurements, it is preferable to conduct FTIR without pyridine to identify the major fingerprint of the samples. The fingerprint of zeolite acidity was located in the range of 1800–1400 cm^{-1}.[25] In this study, four bands were identified in this area, namely at around 1630, 1550, 1485 and 1450 cm^{-1}, as presented in Fig. 4(a). From these peaks, the band at 1550 cm^{-1} corresponds to pyridinium adsorption on the Brønsted acid, while the coordination between pyridine and the Lewis acid site appears at 1450 cm^{-1}. The bands at 1630 and 1485 were assigned to pyridine that adsorbed on both Brønsted and Lewis acid sites. In this study, the amount of Brønsted and Lewis acid sites decreased after ion-exchange and steam treatments due to the removal of a proton on the bridged hydroxyl groups and Al in the zeolitic framework. Then, the –OH stretching was evaluated *via* FTIR spectroscopy, as shown in Fig. 4(b); generally, there are three bands in the region of 3730–

3600 cm^{-1}. In this study, the observed bands consisted of strong, medium, and low intensity at 3745, 3680 and 3600 cm^{-1}, which correspond to the terminal silanol (Si–OH), extra-framework Al–OH and bridging Si–OH–Al. The band at 3680 cm^{-1} decreased significantly in H–Y10 and S–Y10 attributed to the decreasing amount of extra-framework Al–OH, which aligned with FTIR pyridine leading to Al removal, thus decreasing the overall acidity.

The acidic nature of the catalysts was determined with NH$_3$-TPD, and the result is depicted in Fig. 5. In general, two peaks corresponding to strong and weak acid sites appear at high and low temperatures, respectively.[26] In this study, only one peak appeared at around 70–470 °C, which is the region for medium and weak acid sites. This could be explained by the high alumina content. After the steam treatment, less acidity was clearly observed as results of the acid site removal by
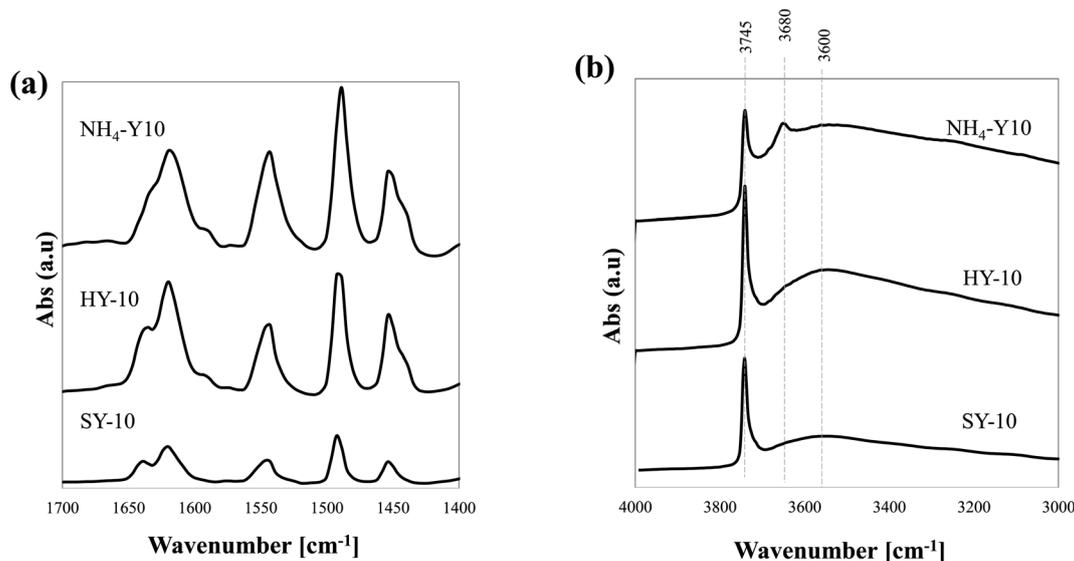
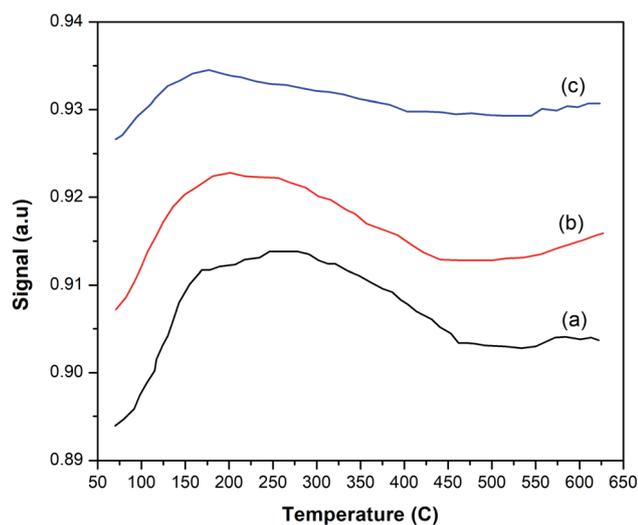Fig. 4   (a) Pyridine FTIR and (b) FTIR-OH.

Fig. 5   NH$_3$TPD of (a) NH$_4$–Y10 (b) HY-10 (c) SY-10.

dealumination. Accordingly, the acidity modification resulted in a decreasing ratio trend of Brønsted acid sites to Lewis acid sites, signifying acid evolution after treatment.

Solid state NMR was used to identify the location of an element after specified treatment. ^{27}Al MAS NMR is a promising method to verify the characteristics of Al such as position, geometry and structure.[27] In this study, ^{27}Al MAS NMR was carried out on all sample, and the results are presented in Fig. 6. There are three peaks attributed to Al characteristics in the solid state NMR namely, at chemical shifts of 0, 35 and 60 ppm, which correspond to octahedral (extra-framework) (Al VI), pentahedral (framework) (Al V) and tetrahedral (framework) (Al IV).[28] We observed drastic evolution to Al for each treatment. Initially, the Al in the parent Na–Y10 was located only in the tetrahedral framework as indicated by its high intensity at

around chemical shift of 60 ppm. The treatment then lowered the area under the tetrahedral framework, which was followed by the corresponding broadening of the area at 0 and 35 ppm assigned to the evolution of a large fraction of Al in the tetrahedral framework. The decreasing proportion of Al IV was an indication to its amorphization, while the enhanced peaks of Al V and Al VI were assigned to framework distortion.[29] The changes observed on the ^{27}Al MAS NMR analysis confirmed the occurrence of Al species leaching and transfer after the treatments. During the process, water molecules from steam was also perceived to attack the acid sites, leading to the permanent removal of Al species and causing nanozeolite-Y crystal distortion.[30] As depicted in Fig. 6(b), Al was mainly located in the tetrahedral sites, but then migrated to the octahedral region after alumina extraction. Additionally, the existence of Al V exposed possible interaction during the treatment that also affected the structure of nanozeolite Y. The treatment may cause the formation of several Al species such as Al^{3+}, Al (OH)$_2$ and AlO$^+$ that were previously reported to increase acidity,[31] and were confirmed with an acidity test in this study as presented in Table 1.

Catalytic testing and stability study

The catalytic evaluation was carried out using S–Y10 catalysts in dodecane cracking and the results are presented in Fig. 7. It was observed that the product mainly consists of gas with a small portion of naphtha. The total gas yield was *ca.* 80% with 50% total olefins yield, slightly higher than BEA zeolites.[32] The produced olefins included *ca.* 22% ethylene, 17% propylene and 11% butylene.

The catalytic activities of the catalyst were also conducted in several space of velocities and temperatures, which are shown in Fig. 8. As shown in Fig. S3,† the un-catalyzed reactions of dodecane conversion are only at 40–45% indicating the crucial role of catalytic cracking over thermal cracking. The dodecane
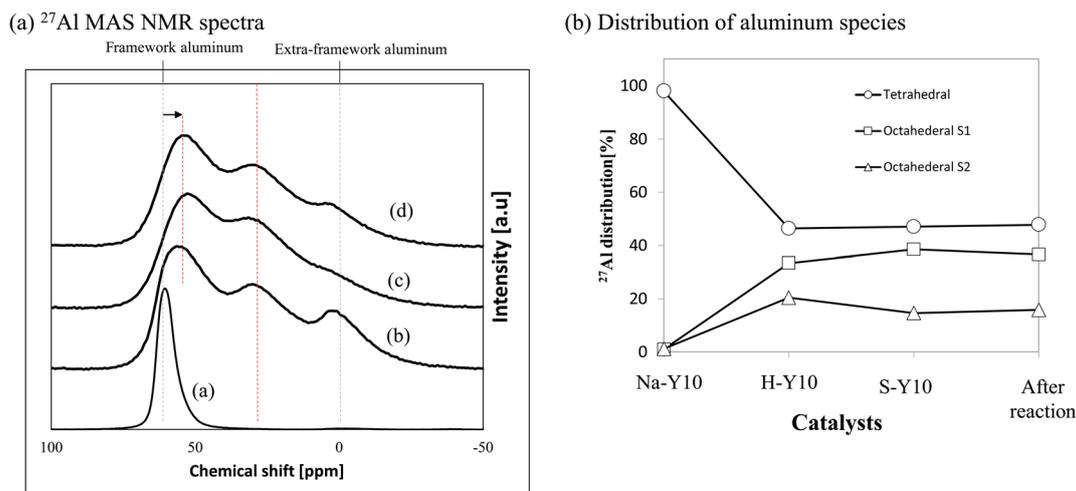
Fig. 6 (a) ^{27}Al MAS NMR spectra of nanozeolite of (a) NH$_4$–Y10 (b) HY-10 (c) after reaction (d) SY-10 (b) Al species distribution in the catalysts.
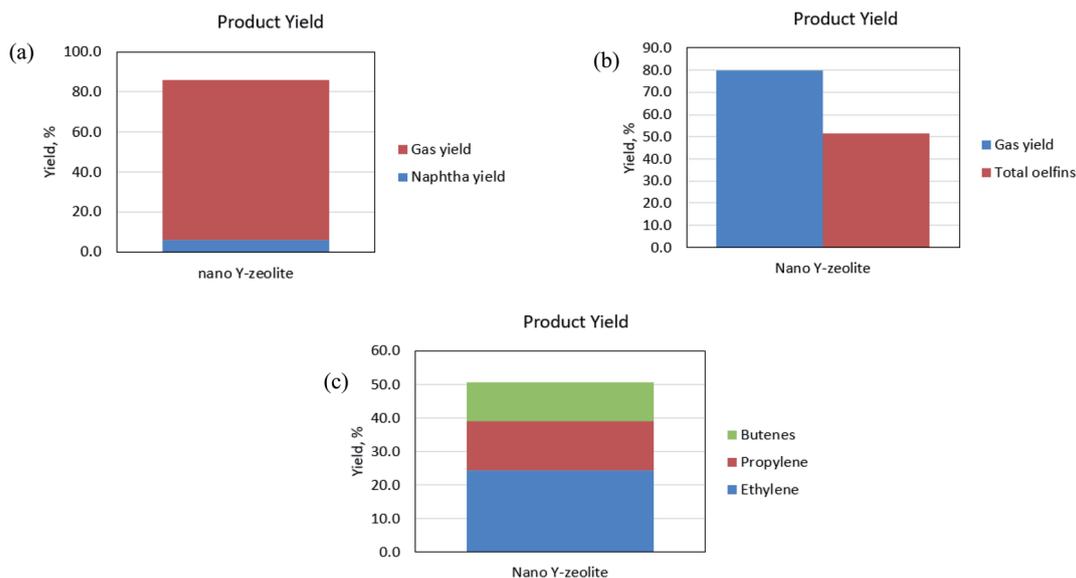

Fig. 7 (a) Yield to naphtha (b) yield to olefins and (c) olefins distributions.

conversion decreased with the increase the space velocities. The active sites of the nanozeolite-Y may be not be sufficient to accommodate high amounts of dodecane; thus, some unreacted dodecane remained in the catalyst reactor.[33] Moreover, increasing the temperature, increased the conversion, indicating an endothermic reaction as typical of catalytic cracking reactions.[34,35] The activation energy of nanozeolite Y was at 138 kJ mol^{-1}, as presented in Fig. S4,† which decreased significantly from that of pure dodecane at 257 kJ mol^{-1}.[36] The catalyst exhibited competing activity with previous reports, as presented in Table S1.†

The reaction in paraffin cracking is mainly based on a monomolecular reaction where the paraffin chain is protonated by a Brønsted acid site and forms a carbenium ion.[37,38] These intermediates lead to the formation of lower paraffins and olefins with the simultaneous regeneration of the acid site.

The produced olefins may transform to aromatics by the elimination of H$^-$ and H$^+$, which could be followed by hydride transfer that possibly alters olefins to other types of paraffins. The hydride transfer may also occur on the Lewis acid site, which leads to the generation of lighter paraffins and olefins. Fig. 9 shows the proposed reaction mechanism to nanozeolite-Y after the treatment. The product distribution in this study was mainly gas yield with only a low content of naphtha as an indication of the Brønsted acid route. In addition, the existence of C$_3$–C$_4$ olefins was perceived as a secondary reaction, which may occur through bimolecular cracking reactions.[8] Since the hydride transfer of nanozeolite is limited, the produced olefins may experience cyclization to aromatics, thus generating coke.[39]

The generated coke was investigated in this study *via* thermal gravimetric analysis (TGA). Coke as one of the influencing factors in catalyst deactivation originates from the
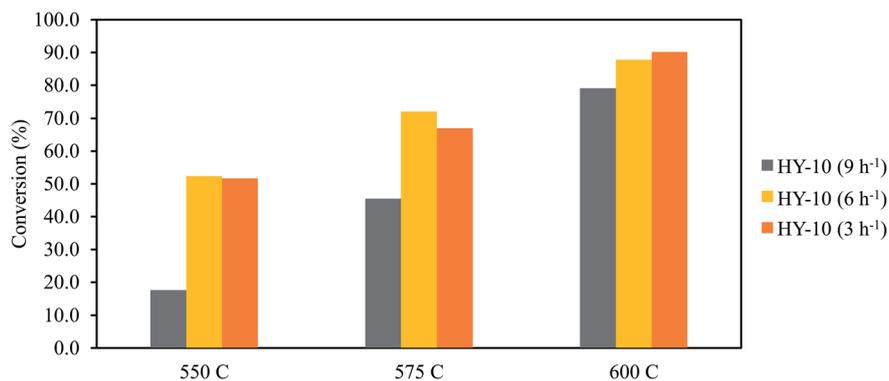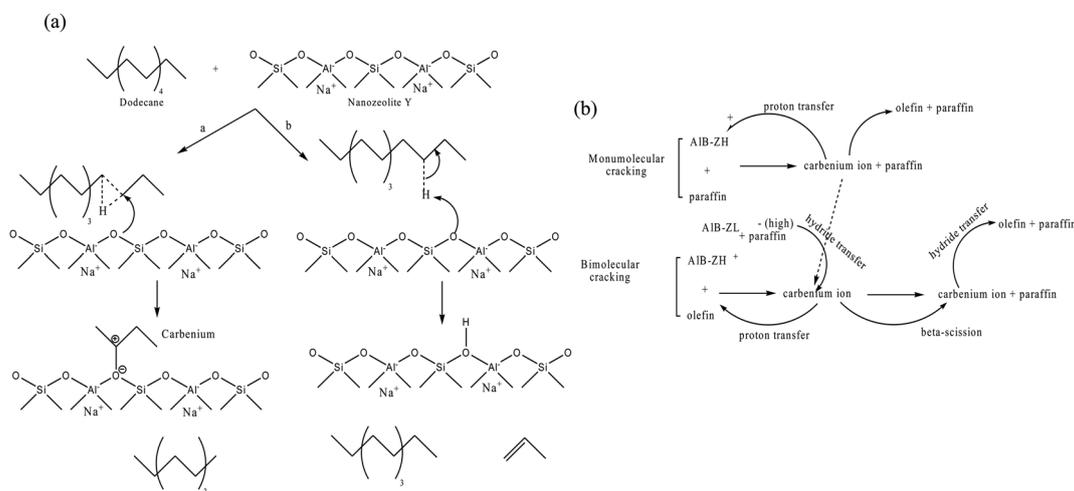
Fig. 8 Effect of space velocity and temperature.

Fig. 9 (a) The proposed dodecane conversions to olefins[38] and (b) hydride transfers.[8]

catalyst or side reactions. From the TGA analysis for S–Y10 catalyst, as presented in Fig. 10, the amount of carbon content was *ca.* 9%. The weight loss around 50–300 °C could be attributed to the loss of water physically and chemically bound to the

Fig. 10 TG analysis of Y10 coke sample.

zeolite sample. Meanwhile, the weight loss in the range of 300–650 °C was perceived as coke formation.[40] Based on the FTIR spectroscopy results of pyridine, the catalyst exhibits almost equivalent Brønsted and Lewis acid sites. The Brønsted acid sites promote paraffin cracking with a high tendency to form coke at a high temperature (500 °C).[41] The Lewis acid sites were attributed to the production of olefins and aromatics, which are identified as secondary reactions. The aromatic groups may be trapped inside the nanozeolite framework that decreased the porosity at the initial formation of coke. Thus, dehydrogenation became broader in the zeolite framework and increased the catalyst deactivation.[42]

Conclusion

The increasing demand for olefins has presented a challenge to researchers to develop more advanced techniques with alternative resources. *n*-Dodecane is considered as a feedstock intersection between heavy oil and biomass pyrolysis, which seems promising for olefin production. In this study, the as-prepared nanozeolite has a crystal size of 10 nm in the absence of a templating agent. The parent zeolite was modified by ionic exchange, followed by either calcination or steam
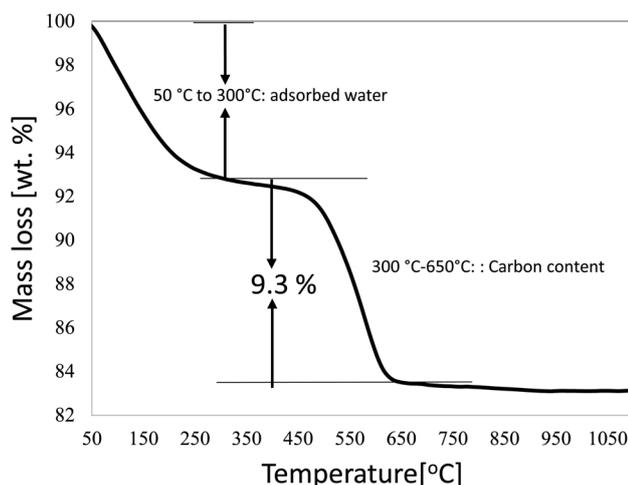
treatment. This modification led to the acid evolution of the sample, which exhibited weak and medium acidity. In addition, the treatment also altered the structure of Al from a complete tetrahedral to a combination of octahedral and tetrahedral. The steam catalytic cracking (SCC) of dodecane over S–Y10 catalysts showed a high yield of olefins with the major portion being ethylene. However, the sample showed a moderate content of coke as observed from the TGA analysis.

Conflicts of interest

The authors declare no competing financial interest.

Acknowledgements

References

1 M. Ghavipour, A. S. Mehr, Y. Wang, R. M. Behbahani, S. Hajimirzaee and K. Bahrami, *RSC Adv.*, 2016, **6**, 17583–17594.

2 A. Akah and M. Al-Ghrami, *Appl. Petrochem. Res.*, 2015, **5**, 377–392.

3 U. Khalil, O. Muraza, H. Kondoh, G. Watanabe, Y. Nakasaka, A. Al-Amer and T. Masuda, *Fuel*, 2016, **168**, 61–67.

4 O. Muraza and A. Galadima, *Fuel*, 2015, **157**, 219–231.

5 G. W. Huber and A. Corma, *Angew. Chem., Int. Ed.*, 2007, **46**, 7184–7201.

6 T. Imam and S. Capareda, *J. Anal. Appl. Pyrolysis*, 2012, **93**, 170–177.

7 K. Kon, W. Onodera, S. Takakusagi and K.-i. Shimizu, *Catal. Sci. Technol.*, 2014, **4**, 3705–3712.

8 U. J. Etim, P. Bai, Y. Wang, F. Subhan, Y. Liu and Z. Yan, *Appl. Catal., A*, 2019, **571**, 137–149.

9 X. Hou, Y. Qiu, X. Zhang and G. Liu, *RSC Adv.*, 2016, **6**, 54580–54588.

10 A. A. Dabbawala, I. Ismail, B. V. Vaithilingam, K. Polychronopoulou, G. Singaravel, S. Morin, M. Berthod and Y. Al Wahedi, *Microporous Mesoporous Mater.*, 2020, **303**, 110261.

11 W. Q. Jiao, W. H. Fu, X. M. Liang, Y. M. Wang and M.-Y. He, *RSC Adv.*, 2014, **4**, 58596–58607.

12 L. Cao, H. Hao and P. K. Dutta, *Microporous Mesoporous Mater.*, 2018, **263**, 62–70.

13 S. Mintova, J.-P. Gilson and V. Valtchev, *Nanoscale*, 2013, **5**, 6693–6703.

14 G.-T. Vuong, V.-T. Hoang, D.-T. Nguyen and T.-O. Do, *Appl. Catal., A*, 2010, **382**, 231–239.

15 H. M. Radman, A. A. Dabbawala, I. Ismail, Y. F. Alwahedi, K. Polychronopoulou, B. V. Vaithilingam, G. P. Singaravel, S. Morin, M. Berthod and S. M. Alhassan, *Microporous Mesoporous Mater.*, 2019, **282**, 73–81.

16 M. H. M. Ahmed, T. Masuda and O. Muraza, *Fuel*, 2019, **258**, 116034.

17 S. Matsuura, T. Hashimoto and A. Ishihara, *J. Porous Mater.*, 2021, **28**, 1935–1944.

18 H. Liu, Z. Diao, G. Liu, L. Wang and X. Zhang, *J. Porous Mater.*, 2017, **24**, 1679–1687.

19 H. Awala, J.-P. Gilson, R. Retoux, P. Boullay, J.-M. Goupil, V. Valtchev and S. Mintova, *Nat. Mater.*, 2015, **14**, 447.

20 F. Ferreira Madeira, K. Ben Tayeb, L. Pinard, H. Vezin, S. Maury and N. Cadran, *Appl. Catal., A*, 2012, **443–444**, 171–180.

21 M. A. Camblor, A. Corma, A. Mifsud, J. Pérez-Pariente and S. Valencia, in *Studies in Surface Science and Catalysis*, ed. H. Chon, S.-K. Ihm and Y. S. Uh, Elsevier, 1997, vol. 105, pp. 341–348.

22 M. V. Landau, L. Vradman, V. Valtchev, J. Lezervant, E. Liubich and M. Talianker, *Ind. Eng. Chem. Res.*, 2003, **42**, 2773–2782.

23 A. Ates and C. Hardacre, *J. Colloid Interface Sci.*, 2012, **372**, 130–140.

24 H. Chen, J. Wydra, X. Zhang, P.-S. Lee, Z. Wang, W. Fan and M. Tsapatsis, *J. Am. Chem. Soc.*, 2011, **133**, 12390–12393.

25 M. A. Sanhoob, U. Khalil, E. N. Shafei, K.-H. Choi, T. Yokoi and O. Muraza, *Fuel*, 2020, **263**, 116624.

26 F. Benaliouche, Y. Boucheffa, P. Ayrault, S. Mignard and P. Magnoux, *Microporous Mesoporous Mater.*, 2008, **111**, 80–88.

27 D. Ma, F. Deng, R. Fu, X. Han and X. Bao, *J. Phys. Chem. B*, 2001, **105**, 1770–1779.

28 M. Gackowski, J. Podobiński and M. Hunger, *Microporous Mesoporous Mater.*, 2019, **273**, 67–72.

29 N. Cui, H. Guo, J. Zhou, L. Li, L. Guo and Z. Hua, *Microporous Mesoporous Mater.*, 2020, **306**, 110411.

30 S. Greiser, P. Sturm, G. J. G. Gluth, M. Hunger and C. Jäger, *Ceram. Int.*, 2017, **43**, 2202–2208.

31 J. Huang, Y. Jiang, V. R. R. Marthala, B. Thomas, E. Romanova and M. Hunger, *J. Phys. Chem. C*, 2008, **112**, 3811–3818.

32 G. A. Nasser, M. H. M. Ahmed, M. A. Firdaus, M. A. Sanhoob, I. A. Bakare, E. N. Al-Shafei, M. Z. Al-Bahar, A. N. Al-Jishi, Z. H. Yamani, K.-H. Choi and O. Muraza, *RSC Adv.*, 2021, **11**, 7904–7912.

33 A. Gutiérrez, J. M. Arandes, P. Castaño, M. Olazar, A. Barona and J. Bilbao, *Fuel Process. Technol.*, 2012, **95**, 8–15.

34 B.-G. Park and K.-H. Chung, *Mol. Catal.*, 2018, **461**, 80–85.

35 Y. Ji, H. Yang and W. Yan, *Fuel*, 2019, **243**, 155–161.

36 G. Liu, Y. Han, L. Wang, X. Zhang and Z. Mi, *Energy Fuels*, 2008, **22**, 3960–3969.

37 X. Hou, N. Ni, Y. Wang, W. Zhu, Y. Qiu, Z. Diao, G. Liu and X. Zhang, *J. Anal. Appl. Pyrolysis*, 2019, **138**, 270–280.

38 T. Tago, H. Konno, Y. Nakasaka and T. Masuda, *Catal. Surv. Asia*, 2012, **16**, 148–163.

39 L. Emdadi, L. Mahoney, I. C. Lee, A. C. Leff, W. Wu, D. Liu, C. K. Nguyen and D. T. Tran, *Appl. Catal., A*, 2020, **595**, 117510.

40 M. Siddiqui, S. Holmes, H. He, W. Smith, E. Coker, M. Atkins and I. Kozhevnikov, *Catal. Lett.*, 2000, **66**, 53–57.

41 S. Gao, S. Xu, Y. Wei, Q. Qiao, Z. Xu, X. Wu, M. Zhang, Y. He, S. Xu and Z. Liu, *J. Catal.*, 2018, **367**, 306–314.

42 Y. Song, Q. Zhang, Y. Xu, Y. Zhang, K. Matsuoka and Z.-G. Zhang, *Appl. Catal., A*, 2017, **530**, 12–20.